Combined Effects of Mass Addition and Nose Bluntness on Boundary-Layer Transition

JOSEPH G. MARVIN* AND CLIFFORD M. AKIN†
NASA Ames Research Center, Moffett Field, Calif.

Transition measurements on a 5° half-angle cone, obtained from heat-transfer data, are presented. The cone, consisting of a short solid tip (sharp or blunt) followed by a uniformly porous section, was tested in the Ames 3.5-ft Wind Tunnel at $M_\infty = 7.4$ and freestream Reynolds numbers of 3×10^6, 4.7×10^6, and 7.8×10^6 based on model length. The effects of argon, air, and helium injection (mass rates between 0 and 2.5% of freestream rates) through the porous skin are determined. A significant decrease in transition Reynolds number was observed with increasing mass injection. The magnitude of the decrease is shown to depend on injection rate and molecular weight. For the same mass injection rate, the lighter injectant resulted in a greater decrease. Small nose bluntness moved transition location rearward, but the amount it moved depended on the injection rate and molecular weight. At the highest injection rates, transition location was the same as for the sharp cone.

Nomenclature

A = area
a = model skin thickness
c = model material specific heat
F = injection parameter obtained from $1.3\int_L^{xt} m\, dA/\rho_\infty u_\infty (A_B)_t$
$\bar{F}$ = average injection parameter, $1.3\, \bar{m} A_p/\rho_\infty u_\infty A_B$
L = length of nonporous section from cone apex to beginning of porous section (see Fig. 2)
m = mass injection rate normal to the surface per unit area
$\bar{m}$ = average mass injection rate normal to the surface per unit area obtained by dividing the total mass per unit time by the porous area
M = Mach number
$\mathfrak{M}$ = molecular weight
$\dot{q}$ = heat-transfer rate
r = distance along the normal from axis to cone surface
R_N = nose radius
Re = Reynolds number based on local conditions
Re_∞ = Reynolds based on freestream conditions
S = dimensionless length along porous section, x/L
T = temperature
t = time
u = streamwise velocity
x = distance along surface from cone apex (see Fig. 2)
δ^* = displacement thickness
Φ = azimuthal angle to conical ray
σ = cone semivertex angle
ρ = density
$\bar{\rho}$ = model material density
μ = viscosity

Subscripts

B = cone base
b = blunt tip
g = injectant gas in inner cone
i = injectant
l = based on total length of sharp cone
o = stagnation
p = porous section
s = sharp tip
t = at transition
w = wall
x = based on surface length from sharp cone apex
θ = based on momentum thickness
∞ = freestream

Presented as Paper 69-706 at the AIAA 2nd Fluid and Plasma Dynamics Conference, San Francisco, Calif., June 16–18, 1969; submitted June 16, 1969; revision received November 10, 1969. The authors are grateful to C. Stalmach of L.T.V., Dallas, Texas, for his assistance in calibration and his suggestions regarding porous material selection and welding techniques.

* Assistant Chief, Fluid Mechanics Branch, Thermo- and Gas-Dynamics Division. Associate Fellow AIAA.
† Research Scientist.

Introduction

BLUNTNESS can be an effective means of delaying transition on slender cones.[1–3] Reference 1 demonstrated that as bluntness is increased, the transition location first moves rearward on the cone surface until an optimum bluntness is achieved and thereafter transition moves forward rapidly to the blunt body position. References 1 and 2 suggest the rearward movement of transition follows the unit Reynolds number change along the boundary-layer edge caused by the entropy layer from the curved shock wave, since the transition Reynolds number is essentially fixed at the sharp cone value. Reference 3 indicates this unit Reynolds number dependence may not be correct and that further rearward movement of transition may be possible before the optimum bluntness is achieved. Although the optimum bluntness and its dependence on Mach number have not been determined, it is well established that small bluntness can delay transition in the absence of boundary-layer mass addition. A natural question that arises is whether this phenomenon can be used to advantage on bodies undergoing boundary-layer mass addition which occurs in many practical situations. Very little is known regarding the influence of mass addition on transition. Limited experimental data on sharp cones with injection through a porous skin[4,5] show transition to occur sooner. More recent data for ablating sharp cones[6,7] are less definitive; some data[6] show little effect of ablation, probably because the amount of laminar ablation was small, and other data[7] with more laminar ablation show transition occurring sooner. The extent to which bluntness promotes or delays the onset of transition in the presence of mass addition has not been studied. The experimental results described in this paper were obtained to establish the trends of transition with the combined effects of mass addition and nose bluntness.

Most practical situations involving mass addition occur with ablation systems which respond directly to the heating environment. However, experimental studies of transition on ablating shapes are difficult to perform and their interpretation is subject to many uncertainties related to the response of the material to the heating environment. To

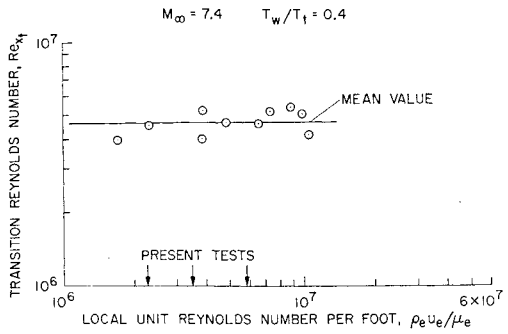

Fig. 1 Transition Reynolds number on a 5° nonporous model as a function of local unit Reynolds number.

circumvent such difficulties and uncertainties the present tests were performed using forced injection through a uniform porous model surface. While sacrificing exact simulation of the usual ablation mass distribution with axial location, this technique allows the injection rate and molecular weight to be varied in a controlled, known manner and makes the prediction of laminar boundary-layer parameters ahead of transition, which might be used for correlation purposes, more readily calculable. The injection rate was varied over a practical range of interest for ablation on slender cones (mass rates between 0 and 2.5% of the freestream rates) and the molecular weight was varied between 4 and 40. Because little is known regarding transition on sharp cones with mass addition, this phenomenon will be considered first. Then the effects of small bluntness will be considered and the movement of transition relative to the sharp cone transition will be shown.

Apparatus and Test Conditions

Facility

The tests were conducted in the Ames 3.5-ft Hypersonic Wind Tunnel at $M_\infty = 7.4$ and $Re_{\infty 1} = 3 \times 10^6$, 4.7×10^6, and 7.8×10^6. Total temperature and pressures were nominally 1500°R and 400 psia, 600 psia, and 1000 psia, respectively. This is a pebble-heated, blowdown tunnel equipped with an axisymmetric contoured nozzle. The nozzle throat section is cooled by helium injection through a slot in the subsonic region.

The facility was recently used to measure the transition Reynolds numbers on a series of nonporous cones.[6] In contrast to most wind-tunnel investigations, no significant unit Reynolds number effect on transition Reynolds number was observed. An example of these results for a sharp 5° cone is shown in Fig. 1 taken from Ref. 6. The transition Reynolds number is essentially independent of local unit Reynolds number along the cone surface. The absence of a unit Reynolds number effect was believed due to the presence of helium in the nozzle boundary layer.[6] It is expected, then, that the changes in transition Reynolds numbers given subsequently are caused by changes in mass injection and nose bluntness only.

Model

The test model was a 5° cone. A sketch indicating the important dimensions is given in Fig. 2. The cone consisted of a solid, removable tip (sharp or blunt) about 3 in. long, a thin, uniform porous section about 16-in. long, and a sting support.

The model construction can be described with the aid of the photographs in Fig. 3. Figure 3a shows a sheet of 0.008-in. thick, sintered, uniformly porous, nickel with chromel-constantan thermocouples spot-welded to one side. The insulated thermocouple leads were tied into a small bundle and laid close to the surface but not touching it. The flat sheet was wrapped over a welding mandrel with its edges butted together and held in place with holding rings. The edges were electron-beam-welded leaving a 0.01 in. seam along the conical ray opposite the thermocouples. (See Fig. 3b.) After the skin was removed from the welding mandrel, rings were beam-welded in both ends of the cone to provide rigidity and mounting supports. The skin was slipped over a perforated, aluminum inner cone (see Fig. 3b) with a 0.153-in. gap between the porous skin and the inner cone. Thin-ring supports were located on the inner cone about 2.5 in. apart to provide additional support for the skin when no gas was passing through it. (The tubes protruding from the rear of the inner cone were used for measuring the inner-cone pressure.) The injectant gas was delivered through a 0.375 in. hole in the rear of the inner cone. A completely assembled model (and the sting support) are shown in Fig. 3c.

Since the thin porous material was easily marked or dented, the handling and assembly of the model required extreme care. The models used during these tests were quite smooth, except for isolated locations where small scratches or dents were visible. It is believed that these imperfections had a minor influence on the transition results, since the no-injection transition Reynolds number agrees with that obtained on a smooth nonporous heat-transfer model.

The results presented subsequently were obtained using three different porous skins. (Manufacturers quoted void fractions of 0.20, 0.30, and 0.40.) The porous skins on the first two models were damaged during the test series due to mechanical failures of the model insert mechanism, and no postrun calibration of skin porosity was made. A postrun calibration of local skin porosity was obtained for the third model. The calibration device is described in Ref. 8. A radiation compensated hot wire device was used to determine the mass flow rate per unit area along conical rays 90° apart. An average mass flow rate was determined from the equation

$$m = \frac{1}{Ap}\int_L^x \int^{360°} m_{\text{meas}}\, r d\Phi dx \qquad (1)$$

The calibration results are shown in Fig. 4 where the mass injection rate from Eq. (1), normalized by the expected average $\bar{m}$, is given as a function of distance along the porous surface. Deviations from the expected rate were independent of the absolute value of $\bar{m}$ and were attributed to nonuniformities in the porous material and to the manner in which the perforated, inner cone delivered the gas.

Test Technique and Data Reduction

Heating Rate Measurements

The test model and sting were mounted on the tunnel insert mechanism located in a chamber used to shield the models from the tunnel flow until steady-state test conditions were reached. Prior to the model insertion, the desired gas injection rate was established through a 0.375-in. tube connecting the model and the gas delivery system located outside the chamber. Air, argon, and helium were used as injectant gases and the total injection rate (lb/sec) was measured with a flowmeter. When steady tunnel flow was established, the model was inserted into the stream and the wall tem-

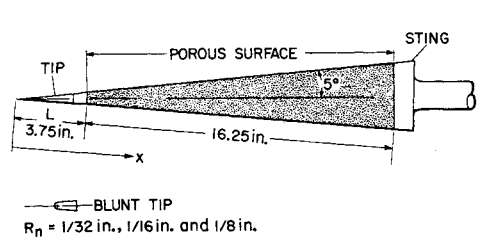

Fig. 2 Test model.

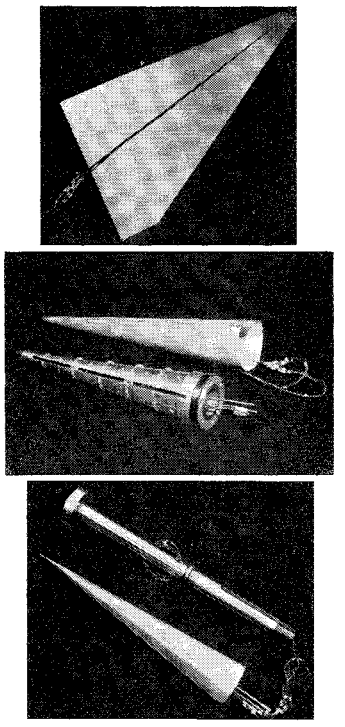

Fig. 3 Photographs showing model construction stages; a) thermocouple installation; b) porous section and inner cone; c) assembled model and sting.

peratures recorded every 0.02 sec on magnetic tape. The test duration was approximately 2 sec, but only the temperature data obtained in the first half-second after insertion were used.

The transient temperature response of the thin porous skin was used to obtain heat-transfer rates. Recorded temperatures were curve fitted and differentiated as a function of time on a digital computer and the heat transfer obtained from the following heat-balance equation:

$$\dot{q} = (\bar{\rho}ca)dT_w/dt + m(T_w - T_g)C_{pg} \qquad (2)$$

[The second term in Eq. (2) accounts for the heat loss from the inner surface of the porous skin if it is assumed that the thin-skin inner and outer temperatures are the same.] The heat loss term was only important for helium injection at high rates, as will be shown later.

Transition Location

The beginning of the transition was determined from the heat-transfer measurements. The heating rates were plotted as a function of distance along the model surface on a log-log scale. An example set of data for a given dimensionless injectant rate is shown in Fig. 5. Straight lines were faired through the data in the manner shown and the intersection of these lines was taken as the location of the beginning of transition. Although this procedure proved satisfactory, it should be pointed out that for some of the higher injectant rates the heat transfer was essentially zero over the portion of the model near the transition location determined from the two intersecting straight lines. Taking into account the uncertainties at the higher injection rates and data accuracy

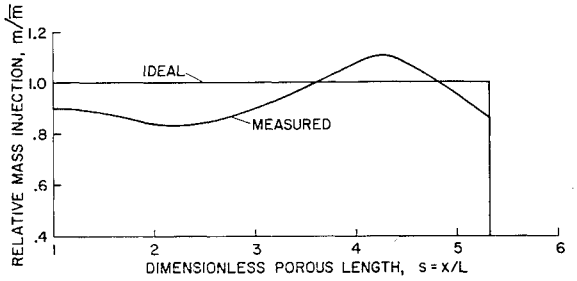

Fig. 4 Relative mass injection rate along porous skin.

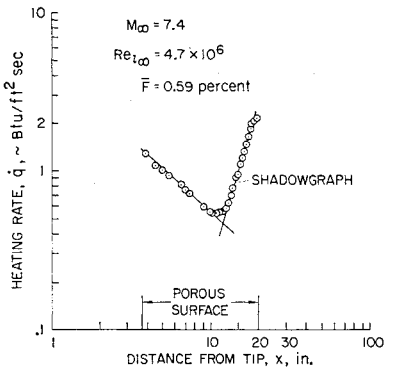

Fig. 5 Determination of transition location for argon injection using measured heat-transfer data.

and repeatability, it has been estimated that transition locations determined in the preceding manner were accurate to within 0.75 in.

Shadowgraphs were also taken during some of the tests. The location and size of the access port limited the shadowgraph field of view and the freestream density level of the tests and the presence of helium in the nozzle boundary layer resulted in rather poor quality shadowgraphs. An example shadowgraph taken along with the heating data in Fig. 5 is shown in Fig. 6. The white line was interpreted as the edge of the laminar boundary layer and the first detectable breakup of this line was interpreted as the location of transition. This transition location was always downstream of the location from the heat-transfer data (e.g., see Fig. 5). The present shadowgraph interpretation is consistent with that reported recently.[7]

Results and Discussion

The first portion of this study is concerned with establishing the effects of mass-transfer rate and injectant composition on the transition location on a sharp cone. After the transition trends with these parameters have been established, the relative effectiveness of nose bluntness is demonstrated by a comparison of blunt-cone transition locations with sharp-cone transition locations.

Sharp Cone

Typical heating distributions

Heating rate distributions over the porous section which show the effects of air, argon, and helium injection for a range of the average injection parameter $\bar{F}$ are presented in Fig. 7. The bars on the helium data represent the magnitude of the heat loss from the back side of the porous skin [see Eq. (2)]. (For air and argon injection the heat losses were negligible because their specific heats are about an order of magnitude smaller.) Where the flow was laminar, the heating rates decreased with distance along the surface. The subsequent increase in heating occurred where the flow was transitional. At the higher injection rates the heating achieved a maximum level in the transition region and then decreased. The flow was interpreted as turbulent beyond this maximum. Increasing the injection rate significantly reduced the heating in the laminar region and, for the highest

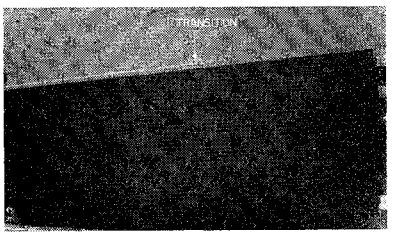

Fig. 6 Shadowgraph showing transition location for test conditions given in Fig. 5.

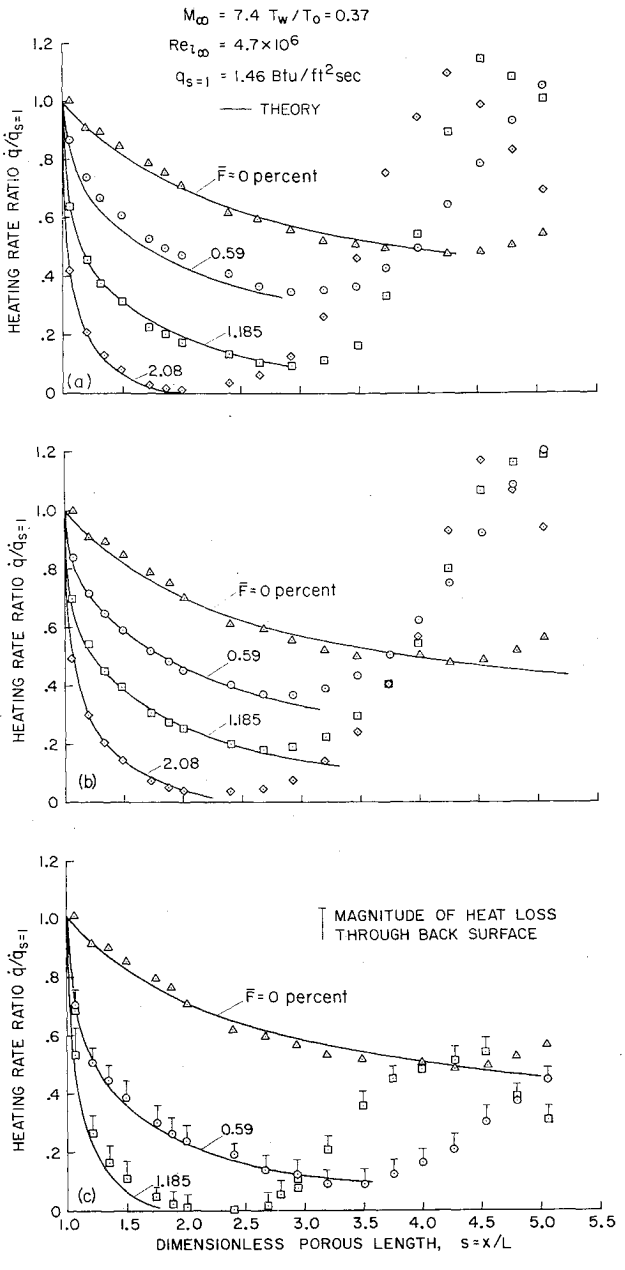

Fig. 7 Effects of injection on heat transfer to a sharp 5° cone; a) air injection; b) argon injection; c) helium injection.

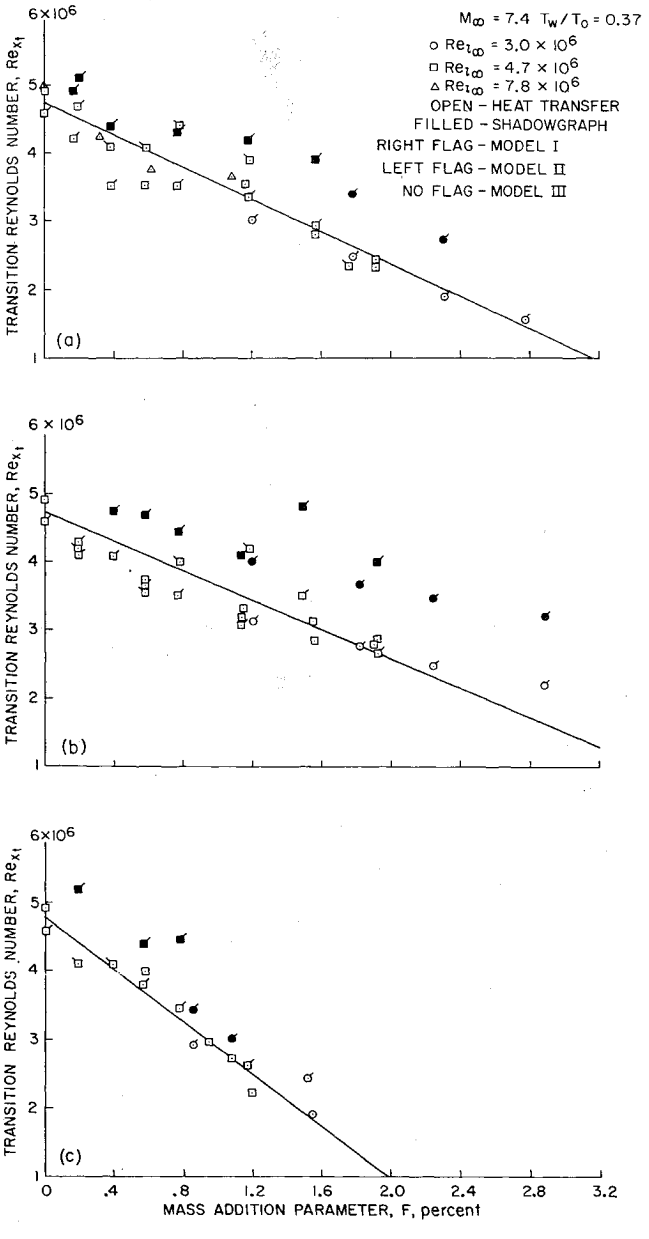

Fig. 8 Effect of injection on transition Reynolds number for a sharp 5° cone; a) air injection; b) argon injection; c) helium injection.

injection rates, the magnitude of the laminar heating was negligible. However, the effect of increasing the injection was to move transition closer to the cone tip with the result that the heating rates downstream in the transition region usually achieved higher values than those for no injection. The relative effectiveness of the injectant gases in reducing heating is evident. For the same injection rate, the reduction was largest with helium and the smallest with argon. Air was somewhat more effective than argon.

Also shown are predicted laminar heating rates. These predictions were obtained from a computer program that solved a finite difference form of the nonsimilar laminar boundary-layer equations including foreign gas injection.[9] The solutions were obtained assuming a constant wall temperature (the average value measured) and the relative injection distribution given in Fig. 4. Also, the injectant-gas temperature was assumed equal to the wall temperature. The boundary-layer edge conditions and surface pressures were obtained from cone tables.[10] The agreement between theory and experiment was good except for helium injection. For the helium injection rates, better agreement can be achieved by considering boundary-layer displacement effects. These effects will be discussed subsequently.

Transition location

The transition Reynolds numbers, obtained using transition locations from heat-transfer data and shadowgraphs and the local unit Reynolds numbers from cone tables,[10] are plotted vs the injection parameter F in Fig. 8. The parameter F is the ratio of the total mass of injected gas in the boundary layer ahead of transition to the total mass of freestream gas passing through an area equivalent to the cone cross section at the transition location.§ Transition

§ The important distinction between F and $\bar{F}$ arises because only the mass addition up to the transition location should be considered. In particular, the distinction would be important when transition was considered on an ablation surface undergoing laminar, transitional, and turbulent heating. The factor 1.3 in the definitions for F and $\bar{F}$ accounts for an error in the injection rates quoted in the original paper.

Reynolds numbers obtained from shadowgraphs were always greater than those from the heat-transfer data. As mentioned before, for no injection, the transition Reynolds number from the heat-transfer data agrees with the mean value shown in Fig. 1 taken from Ref. 6.

The transition Reynolds number is reduced with increasing injection. The reduction is believed to be related to the changes in laminar boundary-layer momentum and energy and corresponding changes in velocity and temperature profiles across the boundary layer caused by injection. For a fixed value of F the transition Reynolds number reduction is found to be a function of injectant gas composition; e.g., compare helium injection with air injection. This difference in reduction is consistent with the well-known fact that for a given injection rate helium causes a greater change in boundary-layer momentum and energy and a corresponding greater change in the velocity and temperature profiles than air. Similar results were reported in Refs. 4 and 5. Obviously, the limit of the Reynolds number decrease with the injection parameter depends on the freestream unit Reynolds number and the length of the nonporous tip. Whether this limit could be reached was not determined. (In these tests transition always occurred downstream of $S = 2$.)

As shown in Fig. 9, the transition Reynolds numbers from the heating data can be correlated in terms of the injection parameter and molecular weight. The correlating parameter was obtained by analytically fitting the data for each injectant gas with linear curves, as shown in Fig. 8, and using their slopes to determine the molecular weight dependence. The exponential dependence on molecular weight ratio turned out to be the same as that used by others to correlate the decrease in laminar skin friction and heat transfer with foreign gas injection.[11] The linear equation expressing the correlation is

$$Re_{x_t} = (Re_{x_t})_{F=0}\left[1 - 0.25\left(\frac{M_{air}}{M_i}\right)^{0.25}F\right] \qquad (3)$$

where F is expressed in percent.

Correlations of transition results on laminar boundary-layer momentum and displacement thickness at transition have been proposed by others for the case of no injection. Momentum thickness is related to the boundary-layer momentum and has physical significance regarding transition. Displacement thickness has been suggested at hypersonic Mach numbers because this thickness is nearly equivalent to the height in the boundary layer where disturbances propagate sonically with respect to the freestream at the boundary-layer edge. For the present transition results with injection neither thickness provided correlation of all the data for the complete range of F but the results using momentum thickness are interesting and worth mentioning.

Transition Reynolds numbers based on momentum thickness calculated using the computer program mentioned previously are presented for several values of F in Fig. 10.

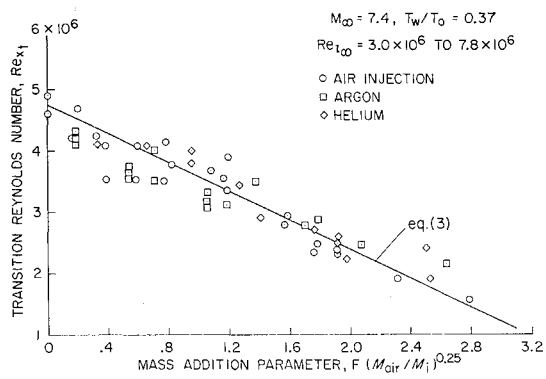

Fig. 9 Correlation of sharp cone transition Reynolds numbers.

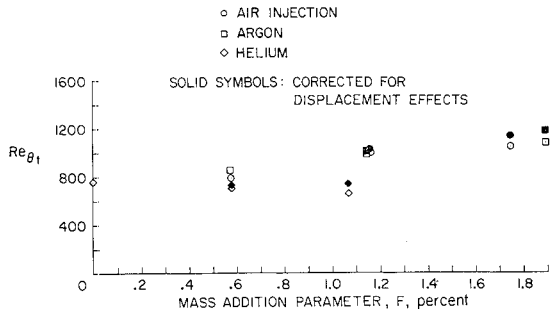

Fig. 10 Transition Reynolds number based on momentum thickness, $Re_{1_\infty} = 4.7 \times 10^6$.

The results indicate that for values of F less than 1.0 the transition Reynolds number could be approximated by the no injection value. For larger values of F, the transition Reynolds numbers increase significantly, except for the helium point at $F = 1.08$. For the higher injection rates displacement effects cause increases in pressure along the cone porous surface and changes in boundary-layer edge velocity and temperature. Since these changes result in decreases in momentum thickness and might alter the results in Fig. 10, displacement effects were estimated using a tangent cone approximation with the effective cone angle[12] given by

$$\sigma_{eff} = \sigma + d\delta^*/dx + m/\rho_e u_e \qquad (4)$$

The last two terms in Eq. (4) were evaluated from boundary-layer solutions assuming sharp-cone edge conditions. Including displacement effects decreased the momentum thickness, but at the same time increased the local unit Reynolds numbers. The net result, given by the solid symbols in Fig. 10, was an increase in momentum-thickness Reynolds number approximately equal to the square root of the increase in local unit Reynolds number. The trend of increasing Re_{θ_t} in Fig. 10 is still obvious. Therefore, using the transition Reynolds number for zero injection would give conservative estimates of the transition location.

Blunt Cone

Nose bluntness introduces an entropy layer which decreases the local unit Reynolds number and Mach number at the boundary-layer edge. For a given freestream Mach number the amount of bluntness and the freestream Reynolds number determine the extent to which these local parameters are reduced and their effectiveness in delaying transition (e.g., see Ref. 1). The additional effects resulting from boundary-layer gas injection will be considered next.

Typical heating distribution

An example of the combined effects of bluntness and injection on the heating distribution along the surface of the test cone is given in Fig. 11 for one Reynolds number. The measured heating rates for air injection have been normalized by the theoretical sharp cone heating rate at $S = 1$ to facilitate comparison. The general behavior of the heating rate with injection is similar to that discussed previously for the sharp cone. However, increasing bluntness has two effects worth noting: first, the heating is reduced in the laminar region and the amount of reduction for $S < 2$ depends on the nose bluntness and the injection rate (e.g., compare $\frac{1}{32}$ and $\frac{1}{8}$-in. results for $\bar{F} = 0.59\%$); second, the distance to transition from the virtual cone apex is increased. The solid lines represent predictions of the laminar heating from the finite difference program. These solutions were obtained assuming a constant wall temperature and the relative injection distribution given in Fig. 4. The surface pressure and boundary-layer edge conditions were obtained from a blunt

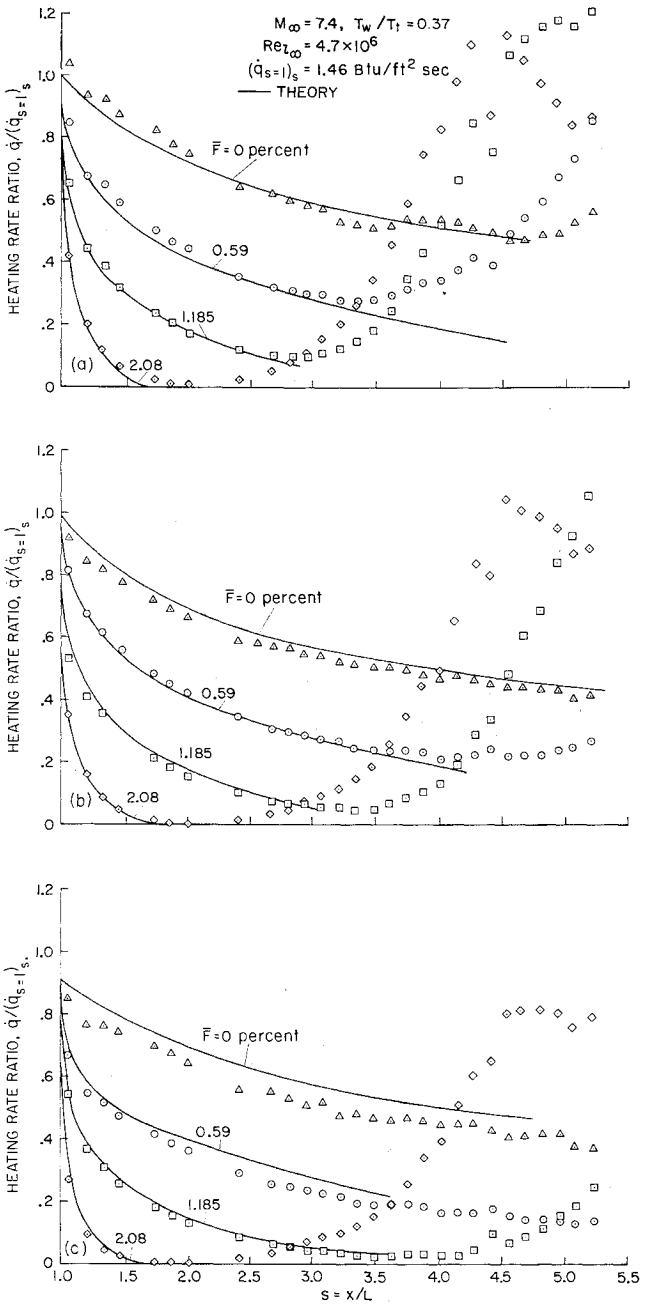

Fig. 11 Effect of air injection on the heating rate to a 5° blunted cone; a) $R_N = \frac{1}{32}$ in.; b) $R_N = \frac{1}{16}$ in.; c) $R_N = \frac{1}{8}$ in.

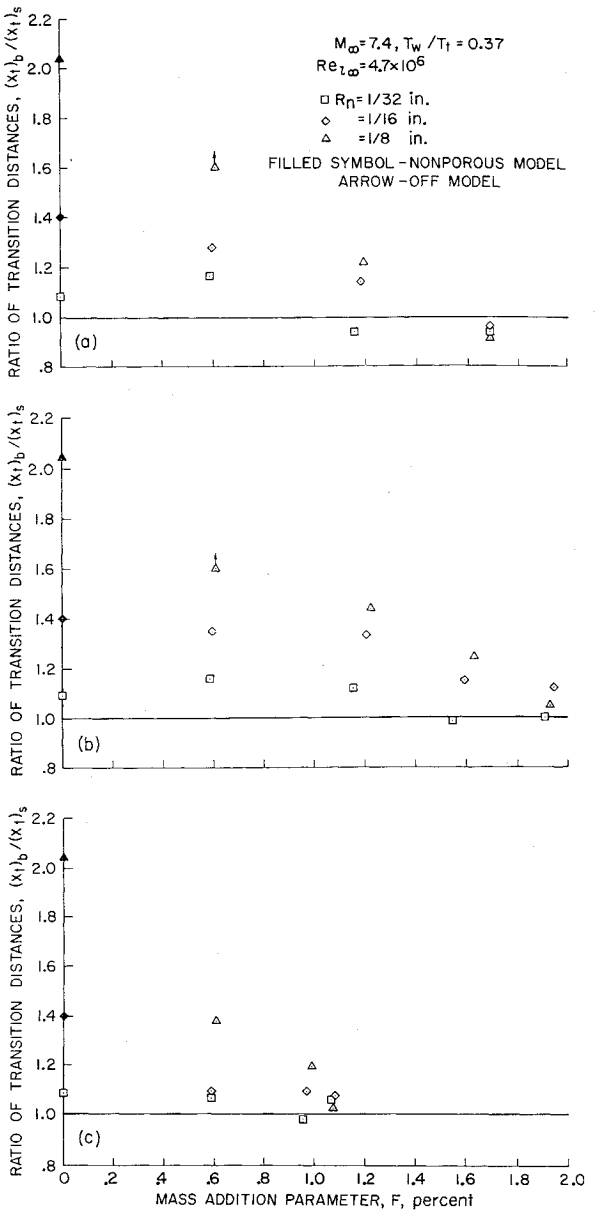

Fig. 12 Effect of bluntness on transition location; a) air injection; b) argon injection; c) helium injection.

body and characteristics solution of the inviscid flow over a blunted 5° cone. No displacement effects have been considered. The agreement of theory and experiment is good. Similar results were obtained for the other injectant gases.

Transition location

The transition locations for the three injectant gases are given in Fig. 12. The distance from the virtual cone apex to the transition location on the blunt cones has been normalized by the sharp cone distance to transition for the same $\bar{m}$ and plotted vs the injection parameter, F. For no injection, transition did not occur on the instrumented portion of the porous model with the $\frac{1}{16}$- and $\frac{1}{8}$-in. nose radii. Therefore, data on a longer solid-wall 5° cone, obtained in the same facility by G. Mateer of Ames, have been plotted. Without injection there is a significant rearward movement of transition location as bluntness is increased. Similar results for small bluntness have been reported in Refs. 1 and 3. As injection increases, however, the relative rearward movement of transition diminishes and the rate at which it diminishes depends on the nose radius and injectant molecular weight. Evidently, the boundary-layer destabilizing effects due to injection are the primary cause of transition and any favorable effects of bluntness are secondary. For a given bluntness, the molecular weight dependence of the relative movement of transition with the injection parameter F can be accounted for approximately by using the parameter, $F(M_{air}/M_i)^{0.25}$. The transition ratios for the $\frac{1}{8}$-in. radius plotted in this manner are shown in Fig. 13. Similar results are obtained for the other nose radii.

For a given Mach number, the extent of the entropy layer over the body depends on the freestream Reynolds number and corresponding boundary-layer growth. Additional data were obtained which show that the foregoing results also depend on the test Reynolds number. Therefore, a quantitative extension of the foregoing results to other freestream Reynolds numbers would require a correlation parameter accounting for this. For no injection, Ref. 1 recommended a correlation based on the entropy layer swallowing distance, and Ref. 3 recommended a correlation based on the distance to the location where disturbances at the boundary-layer

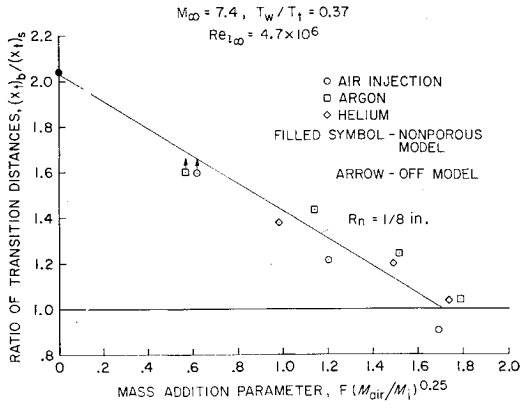

Fig. 13 Correlation of molecular weight dependence of blunt cone transition movement, $R_N = \frac{1}{8}$ in.

edge travel sonically with respect to the flow outside the entropy layer. However, these recommended correlations were not successful when applied to the present data with mass addition because the boundary-layer edge values of velocity, density, and temperature, upon which the swallowing distance or the sonic disturbance distance depend, were not changed significantly when binary injection was accounted for. (The total pressure at various locations behind the shock wave was obtained by equating the mass of air entrained in the boundary layer, determined from the finite difference boundary-layer solutions, to the mass flow through the shock wave. Subsequent expansion to the cone surface pressure uniquely defined the boundary-layer edge conditions.) To be successful, the correlations would also have to include second-order boundary-layer effects and/or a mass-addition parameter, possibly like that used in Fig. 13.

Conclusions

A study of the combined effects of uniform injection and nose bluntness on transition resulted in the following conclusions:

1) The sharp cone transition Reynolds number was decreased significantly with increasing injection rate. The decrease was approximately linear with increasing injection rate and it depended on the injectant molecular weight to the 0.25 power. For a given mass injection rate the lightest injection gas gave the greatest decrease.

2) Small nose bluntness moved the transition location rearward relative to its location on the sharp cone. However, the relative movement depended on the injectant rate and molecular weight. At the highest injection rates where the laminar heating was reduced to a negligible value, the transition location was essentially the same as on the sharp cone.

References

[1] Stetson, K. F. and Rushton, G. H., "A Shock Tunnel Investigation of the Effects of Nose Bluntness, Angle of Attack and Boundary Layer Cooling on Boundary-Layer Transition at a Mach Number of 5.5," *AIAA Journal*, Vol. 5, No. 5, May 1967, pp. 899–902.

[2] Steinback, C. P., "Some Effects of Roughness and Variable Entropy on Transition at a Mach Number of 8," AIAA Paper 67-132, New York, Jan. 1967.

[3] Softley, E. J., "Transition of the Hypersonic Boundary Layer on a Cone. Part II," T.I.S. R68SD14, Oct. 1968, General Electric; also AIAA Paper 69-705, San Francisco, June 1969.

[4] Scott, C. J. and Anderson, G. E., "Boundary Layer Transition With Injection," Research Rept. 151, July 1958, Univ. of Minnesota, Institute of Technology, Rosemount Aeronautical Labs.

[5] Pappas, C. C. and Okuno, A. F., "Measurements of Skin Friction of the Compressible Turbulent Boundary Layer on a Cone With Foreign Gas Injection," *Journal of the AeroSpace Sciences*, Vol. 27, No. 5, May 1960, pp. 321–333.

[6] Mateer, G. G. and Larson, H. K., "Unusual Boundary Layer Transition Results on Cones in Hypersonic Flows," *AIAA Journal*, Vol. 7, No. 4, April 1954, pp. 660–664.

[7] DiCristina, V., "Three Dimensional Laminar Boundary Layer Transition on a Sharp 8° Cone at Mach Number 10," AIAA Paper 69-12, New York, Jan. 1969.

[8] Moore, D. R., Stalmach, C. J., and Pope, T. C., "Dynamic Stability Wind Tunnel Tests of a 10° Cone With Simulated Ablation at $M = 17$," *AIAA Journal*, Vol. 5, No. 8, Aug. 1967, pp. 1377–1385.

[9] Marvin, J. G. and Sheaffer, Y. S., "A Method for Solving the Nonsimilar Laminar Boundary-Layer Equations Including Foreign Gas Injection," TN D-5516, 1969, NASA.

[10] Sims, J. L., *Tables for Supersonic Flow Around Right Circular Cones at Zero Angle of Attack*, SP 3004, NASA, 1964.

[11] Marvin, J. G. and Pope, R., "Laminar Convective Heating and Ablation in the Mars Atmosphere," *AIAA Journal*, Vol. 5, No. 2, Feb. 1967, pp. 240–248.

[12] Grabow, R. M., "Turbulent Boundary Layer Displacement Effects in Hypersonic Flow," TN 34, May 1967, Von Kármán Institute for Fluid Dynamics, Belgium.